

Unique Functional Properties of Mature Adult-Born Neurons in the Mouse Olfactory Bulb

Natalie Fomin-Thunemann,¹ Yury Kovalchuk,¹ Stefan Fink,¹ Astrid Alsema,¹ Nima Mojtahedi,¹ Elizabeta Zirdum,¹ and Olga Garaschuk^{1,*}

¹Institute of Physiology, Department of Neurophysiology, Eberhard Karls University of Tübingen, Tübingen, Germany

*Correspondence: olga.garaschuk@uni-tuebingen.de

<https://doi.org/10.1016/j.stemcr.2020.10.010>

SUMMARY

The rodent olfactory bulb (OB) is continuously supplied with adult-born cells maturing into GABAergic neurons. Using *in vivo* ratiometric Ca²⁺ imaging to readout ongoing and sensory-driven activity, we asked whether mature adult-born cells (mABCs) in the glomerular layer of the bulb become functionally identical to resident GABAergic (Res_{GABA}) neurons. In awake head-restrained mice the two cell populations differed significantly in terms of ongoing spontaneous activity, with 24% of mABCs contributing to a strongly active cell cluster, absent among Res_{GABA} cells. Odor-evoked responses of mABCs were sparse, less reliable, and had smaller amplitudes compared with Res_{GABA} cells. The opposite was seen under anesthesia, with response reliability increasing and response size of mABCs becoming larger than that of Res_{GABA} cells. Furthermore, ongoing activity of mABCs showed increased sensitivity to ketamine/xylazine and was selectively blocked by the antagonist of serotonin receptors methysergide. These functional features of mABCs clearly distinguish them from other OB interneurons.

INTRODUCTION

The rodent olfactory bulb (OB) is continuously supplied with adult-born cells (ABCs). These cells are implicated in odor discrimination; facilitation of the task-dependent pattern separation; short- and long-term olfactory memory; perceptual, associative olfactory, and fear learning (Alonso et al., 2006; Li et al., 2018; Moreno et al., 2009; Pan et al., 2012; Sultan et al., 2010; Valley et al., 2009). They also contribute to innate olfactory behaviors, such as mating, pregnancy, and offspring recognition (Feierstein et al., 2010; Mak et al., 2007; Sakamoto et al., 2011).

Born in the subventricular zone (SVZ), ABCs migrate via the rostral migratory stream (RMS) toward the OB (Ledo et al., 2008). Ninety percent of these cells become inhibitory granule cells (GCs), while 5%–10% become GABAergic periglomerular (PGCs) or short axon cells (SACs) (Ledo et al., 2008), collectively referred to as juxtglomerular cells (JGCs). Not all cells survive for longer time periods (Petreanu and Alvarez-Buylla, 2002). In addition to endogenous and sensory-driven activity (Lin et al., 2010; Petreanu and Alvarez-Buylla, 2002; Yamaguchi and Mori, 2005), centrifugal inputs arising from the olfactory cortex, basal forebrain, dorsal raphe nucleus, and locus coeruleus were shown to promote survival of ABCs (Bauer et al., 2003; Deshpande et al., 2013; Kaneko et al., 2006; Mechawar et al., 2004; Siopi et al., 2016; Whitman and Greer, 2007).

During the pre-integration phase, i.e. after arrival to the glomerular layer (GL) but before the integration therein (Liang et al., 2016), functional properties of adult-born JGCs are well known to differ from those of Res_{GABA} cells. These differences include (1) expression pattern of glutam-

ergic receptors, with ABCs having lower AMPA to NMDA ratios; (2) lower levels of spontaneous activity; (3) higher odor responsiveness; (4) lower response selectivity; and (5) higher structural plasticity (Belluzzi et al., 2003; Grubb et al., 2008; Kovalchuk et al., 2015; Livneh et al., 2009, 2014; Maslyukov et al., 2018; Mizrahi, 2007; Wallace et al., 2017). Immature ABCs are particularly sensitive to environmental influences. Thus, 2–3 weeks old adult-born GCs were more responsive to novel odors than resident GCs but became less responsive over time (Magavi et al., 2005). Consistently, 2–4 weeks old adult-born PGCs showed larger Na⁺ conductance, had higher odor-evoked action potential (AP) firing rates, and responded more broadly to different odorants compared with 8–9 weeks old or resident cells (Belluzzi et al., 2003; Livneh et al., 2014).

As ABCs mature, their AMPA/NMDA ratio increases (Grubb et al., 2008). From 7 to 8 weeks onward the spontaneous and odor-evoked activity as well as odor-selectivity of ABCs becomes more similar to that of resident cells (Kovalchuk et al., 2015; Livneh et al., 2014; Wallace et al., 2017). Dendritic dynamics decreases and stabilizes at age 6–12 weeks (Livneh et al., 2009; Livneh and Mizrahi, 2011). Therefore, ABCs older than 8 weeks are considered mature. However, the key question remains: Do mature ABCs (mABCs) become functionally identical to Res_{GABA} cells, or do they still preserve unique features, thus increasing the substrate for plasticity and functional diversity of interneurons in the adult OB?

By using *in vivo* two-photon Ca²⁺ imaging in awake, head-restrained mice, we compared the functional properties of mABCs and Res_{GABA} cells in the GL of the bulb with





respect to their spontaneous and odor-evoked activity. As anesthesia modifies functional properties of interneurons (Kato et al., 2012; Wachowiak et al., 2013), we used it as a tool to probe for those functional differences, which might not be evident under awake conditions. Finally, we tested whether the centrifugal projections target mABCs and Res_{GABA} cells differently.

RESULTS

Ongoing Neuronal Activity of mABCs in Awake State

To monitor the level of spontaneous ongoing activity in mABCs of wild-type (WT) mice, we infected them with lentiviruses expressing the ratiometric Förster resonance energy transfer-based Ca²⁺ indicator Twitch-2B (Thestrup et al., 2014) (Figure 1A) and calculated a background-corrected ratio of the acceptor to donor fluorophore fluorescence: cpVenus^{CD}/mCerulean3 (hereafter designated as Twitch-2B ratio; Experimental Procedures). Changes in the Twitch-2B ratio correlate with changes in the intracellular free Ca²⁺ concentration ([Ca²⁺]_i) (Palmer and Tsien, 2006), with higher ratios corresponding to higher levels of [Ca²⁺]_i. In awake mice, the mean basal Twitch-2B ratios, measured in the absence of any exogenous stimuli, ranged from 1.44 to 8.44 (Figures 1B and 1C). As expected (Maslyukov et al., 2018), application of the voltage-gated Na⁺ channel blocker tetrodotoxin (TTX) through a slit in the cranial window (Note S1) caused a profound decrease in basal Twitch-2B ratios (Figure 1D). Under TTX, basal ratios of the majority of cells dropped below 2. Thus, in further analyses cells with basal Twitch-2B ratios <2 were considered “non-spiking.” Only 18.2% of mABCs were non-spiking in the awake state.

To accommodate slight ratio changes caused by the background subtraction and to avoid false positive results, we introduced a safety margin between 2 and 2.4. Only cells with mean basal ratios >2.4 were considered “spiking” (see also Figure S1). Cells with ratios 2–2.4 were considered “uncertain.” Using this categorization, 63.1% of mABCs were considered spiking in the awake state. To test the stability of basal ratios of individual cells over time, the latter were measured on the first recording day and re-examined 3 and 6 days later. Some cells showed higher or lower ratios at later time points (Figure 1E), but on a population level we observed a striking stability of mean basal Twitch-2B ratios of mABCs during a week time span (Figure 1F).

Differences in Basal Twitch-2B Ratio between mABCs and Res_{GABA} Cells

As ABCs mature to become GABAergic interneurons, we compared basal Twitch-2B ratios of mABCs and mature Res_{GABA} cells. Res_{GABA} cells were stained by injection of

an adeno-associated virus encoding a Cre-inducible version of Twitch-2B into *Viaat-Cre* mice. *Post-hoc* immunocytochemistry (Supplemental Experimental Procedures) revealed that these cells comprised 23.61% ± 7.92% of tyrosine hydroxylase-positive, 38.46% ± 16.74% of calretinin-positive, and 19.78% ± 5.63% of calbindin-D-28k-positive cells, similar to the composition of the mABC population analyzed in our previous study (Figure S2) (Kovalchuk et al., 2015).

In awake mice, mean basal ratios of Res_{GABA} cells ranged from 1.27 to 6.05 (Figure 2B). Noteworthy, the cumulative distributions of basal ratios were significantly different between mABCs and Res_{GABA} cells (Figure 2C). We also observed a higher fraction of spiking and a lower fraction of non-spiking cells among mABCs (Figure 2D), but these differences did not reach the level of statistical significance ($p = 0.08$, chi-square test). According to Bayesian information criterion the distribution of basal Twitch-2B ratios of Res_{GABA} cells was best fitted with two Gaussians, whereas that of mABCs was best fitted with three Gaussians (Figure 2E). The first two Gaussians (mean ± SD: 1.98 ± 0.07 and 3.2 ± 0.75 for Res_{GABA} cells, and 1.96 ± 0.06 and 2.97 ± 0.39 for mABCs, respectively) were similar for both cell populations. However, the fit of the mABCs dataset contained a third component (arrow in Figure 2E; mean ± SD: 5.56 ± 1.5), which was absent in the Res_{GABA} dataset.

To relate the measured basal Twitch-2B ratios to cell AP firing frequency, we recorded Twitch-2B ratios of Res_{GABA} cells simultaneously with the underlying APs in *in situ* calibration experiments (Figure S1). By injecting steady-state currents, we varied median AP frequency from 2.5 to 57 Hz and corresponding Twitch-2B ratios from 2.3 to 7.6. Fitting the data with the Hill equation returned the following parameters: $R_{\min} = 1.8$, $R_{\max} = 8.5$, half maximal effective concentration = 13.94, and Hill coefficient = 1.47, which are in a good agreement with *in vivo* data obtained in this and previous studies (Maslyukov et al., 2018; Thestrup et al., 2014).

Differences in Odor-Response Properties between mABCs and Res_{GABA} Cells

To compare odor-evoked Ca²⁺ signals of mABCs and Res_{GABA} cells in awake mice, we used ethyl tiglate (ETI), known to activate numerous glomeruli in the dorsal OB (Rokni et al., 2014). ETI evoked reproducible Ca²⁺ transients both in mABCs and Res_{GABA} cells (Figures 3A and 3B). Cells responding at least once in eight trials were termed “responding,” the ones responding in at least five out of eight trials were termed “reliably responding.”

The fractions of reliably responding, non-reliably responding, and non-responding cells differed significantly between mABCs and Res_{GABA} cells, with Res_{GABA} cells

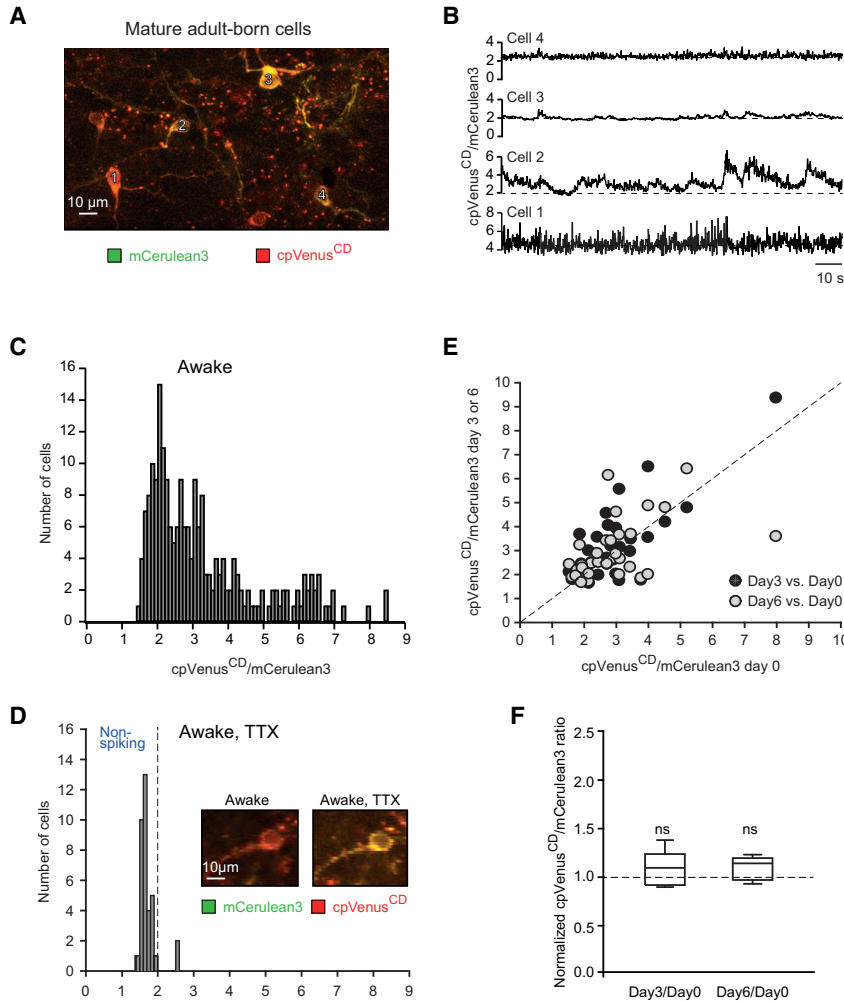


Figure 1. Basal Twitch-2B Ratios of mABCs in Awake Mice

(A) Maximum intensity projection of a 3D stack (90–100 μm below the dura, step 2 μm) showing mABCs (131 days post-injection [DPI]) expressing Twitch-2B. Here and in Figure 2A the image is an overlay of the mCerulean3 (green) and cpVenus^{CD} (red) channels.

(B) Ratio traces recorded in cells marked with respective numbers in (A).

(C) Distribution of mean mABC Twitch-2B ratios under control conditions ($n = 214$ cells, 11 mice).

(D) Distribution of mean mABC Twitch-2B ratios under 5 μM tetrodotoxin (TTX) ($n = 37$ cells, 2 mice). Note that 94.59% of cells had Twitch-2B ratios < 2.0 (vertical broken line). Inset: an overlay image of an mABC before (left, ratio 4.0) and during (right, ratio 1.6) TTX application.

(E) Scatterplot showing the ratios of cells recorded on day 0 (53–71 DPI) plotted against the corresponding ratios recorded 3 or 6 days later ($n = 35$ cells, 5 mice). Diagonal broken line: $y = x$.

(F) Boxplot shows the median (per mouse) normalized Twitch-2B ratios (day 3/day 0 and day 6/day 0). The ratios were not different from one ($p = 0.31$ and 0.19 , respectively, Wilcoxon signed rank test, 5 mice).

having almost twice as many reliably responding cells as mABCs, and mABCs having a three times larger fraction of non-responding cells (Figure 3C). For reliably responding cells, the spread in response amplitude was estimated using the coefficient of variation (CV) (Experimental Procedures). The CVs (Figure 3D) and the odor-evoked maximal ratios (Figure 3F) were similar for mABCs and Res_{GABA} cells. However, the response amplitude of reliably responding mABCs was significantly smaller than that of reliably responding Res_{GABA} cells (Figure 3E). We also observed a significant correlation between the basal and the odor-evoked maximal ratios in both cell groups (Figure 3G).

Effect of Anesthesia on Basal Ca²⁺ Levels of mABCs and Res_{GABA} Cells

Anesthesia has a profound effect on the activity of GABAergic interneurons (Kato et al., 2012; Wachowiak

et al., 2013). We used this fact to test for further differences between mABCs and Res_{GABA} cells. In separate experiments we applied three commonly used anesthesia regimens (medetomidine/midazolam/fentanyl (MMF), ketamine/xylazine (K/X), and isoflurane) and compared the Twitch-2B ratios of the same cells under two conditions: wakefulness and subsequent anesthesia. All anesthesia regimens strongly reduced basal Twitch-2B ratios in mABCs (Figures S3A–S3C). Accordingly, the fractions of spiking and non-spiking cells were almost reversed under the anesthesia (insets in Figures S3A–S3C). To compare the effects of the three regimens, we related the cell's change in the basal ratio (from awake to anesthesia) to the maximal possible change and termed this value “effect size” (Experimental Procedures). The median (per mouse) effect sizes for all anesthesia regimens were large and significantly different from zero (MMF: 56.26%; K/X: 73.73%; isoflurane: 70.86%, $p < 0.01$ for all comparisons, $n = 8$ mice, one-tailed Wilcoxon signed

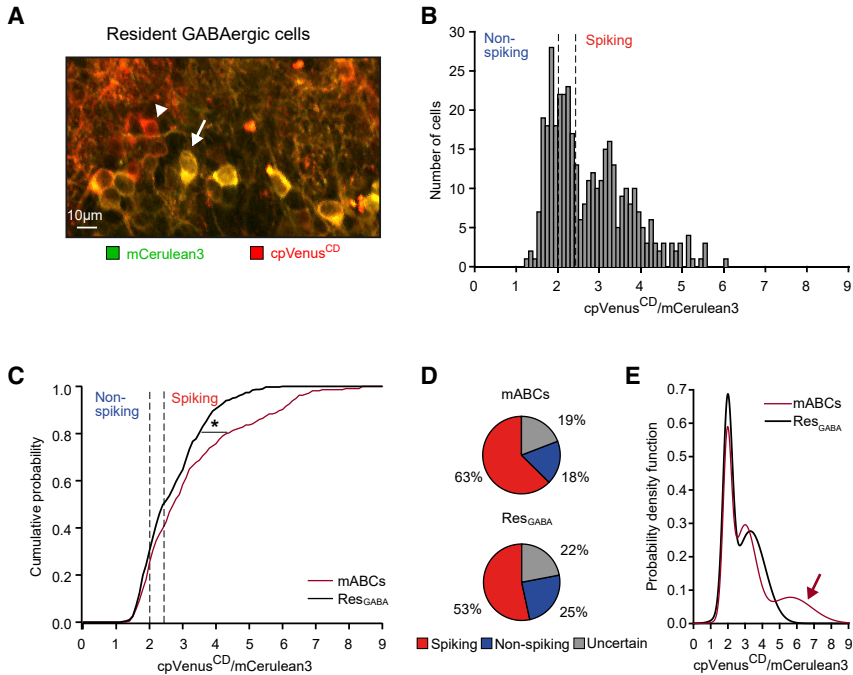


Figure 2. Comparison of Res_{GABA} and mABC Basal Twitch-2B Ratios in Awake Mice

(A) Mean intensity projection image (250 frames) of Res_{GABA} cells (180 DPI). An arrowhead points to a spiking cell (ratio 4.69) and an arrow to a non-spiking cell (ratio 1.6).

(B) Distribution of Twitch-2B ratios in 382 Res_{GABA} cells (n = 5 mice). Here and below vertical broken lines delineate borders between non-spiking and spiking cell populations.

(C) Cumulative probability histograms of Twitch-2B ratios in mABCs and Res_{GABA} cells (*p = 2.5 × 10⁻³, two-sample Kolmogorov-Smirnov test, n = 214 and 382 cells, respectively).

(D) Pie charts showing the fractions of spiking, non-spiking, and uncertain cells among mABCs (top) and Res_{GABA} cells (bottom).

(E) Probability density functions are Gaussian fits of distributions shown in Figures 1C and 2B. The area under the third Gaussian (red arrow) equals 24.1% of the total area under the function.

rank test) with no difference between the three effect sizes (Figure S3D).

In Res_{GABA} cells, anesthesia also strongly reduced the basal Twitch-2B ratios, with cells shifting significantly from spiking to non-spiking state (Figures S4A–S4C). The median (per mouse) effect sizes significantly differed from zero (MMF: 39.73%; K/X: 46.60%; isoflurane: 66.01%, p < 0.05, n = 5 mice, one-tailed Wilcoxon signed rank test). For Res_{GABA} cells, however, the effect sizes of the three regimens were significantly different (Figure S4D).

Next, we compared the effect of anesthesia on mABCs versus Res_{GABA} cells. Under all three regimens basal Twitch-2B ratios of mABCs were lower than those of Res_{GABA} cells (Figures 4A–4C), but the difference reached the level of statistical significance only for K/X anesthesia (Figure 4B). Moreover, the fractions of spiking, non-spiking, and uncertain cells differed between mABCs and Res_{GABA} cells under K/X (inset in Figure 4B) and isoflurane (inset in Figure 4C) anesthesia. Comparing the median (per mouse) effect sizes revealed a significant difference between the three types of anesthesia (Figure 4D). All regimens reduced the basal ratios more strongly in mABCs than in Res_{GABA} cells, but a significant difference was seen only for K/X. Also, at the single-cell level all regimens significantly reduced the basal Twitch-2B ratios in mABCs and Res_{GABA} cells (Figure S5). Under K/X anesthesia, the reduction in mABCs was significantly stronger (Figure S5H).

Odor-Response Properties of mABCs and Res_{GABA} Cells under Anesthesia

Next, we compared the odor-evoked responses of mABCs and Res_{GABA} cells under MMF anesthesia, under which basal Twitch-2B ratios in both cell types were similar (Figure 4A), thus assuring comparable recording conditions. Cell responses were first measured in awake state and then re-examined under MMF anesthesia (Figure 5). Similar to data obtained in awake mice (Figure 3), the fractions of reliably responding, non-reliably responding, and non-responding cells differed significantly between mABCs and Res_{GABA} cells (Figure 5C). Going from awake to anesthesia, the fraction of reliably responding mABCs increased, while that of Res_{GABA} cells decreased but the observed differences did not reach the level of statistical significance (p = 0.11 and 0.12, n = 83 mABCs and n = 222 Res_{GABA} cells, McNemar-Bowker test).

The CVs in mABCs and Res_{GABA} cells were similar under MMF anesthesia (Figure 5D). The response amplitudes also showed the overall similarity (Figure 5E), but comparison of cells with ΔR/R amplitudes above 200% revealed a significant difference (p = 0.04, Kolmogorov-Smirnov test, n = 15 mABCs and n = 41 Res_{GABA} cells). Consistently, the odor-evoked maximal ratios were significantly higher in mABCs (Figure 5F). While Res_{GABA} cells maintained a linear relationship between the basal and the corresponding maximal ratios (Figure 5G), mABCs lost this relationship under MMF anesthesia.

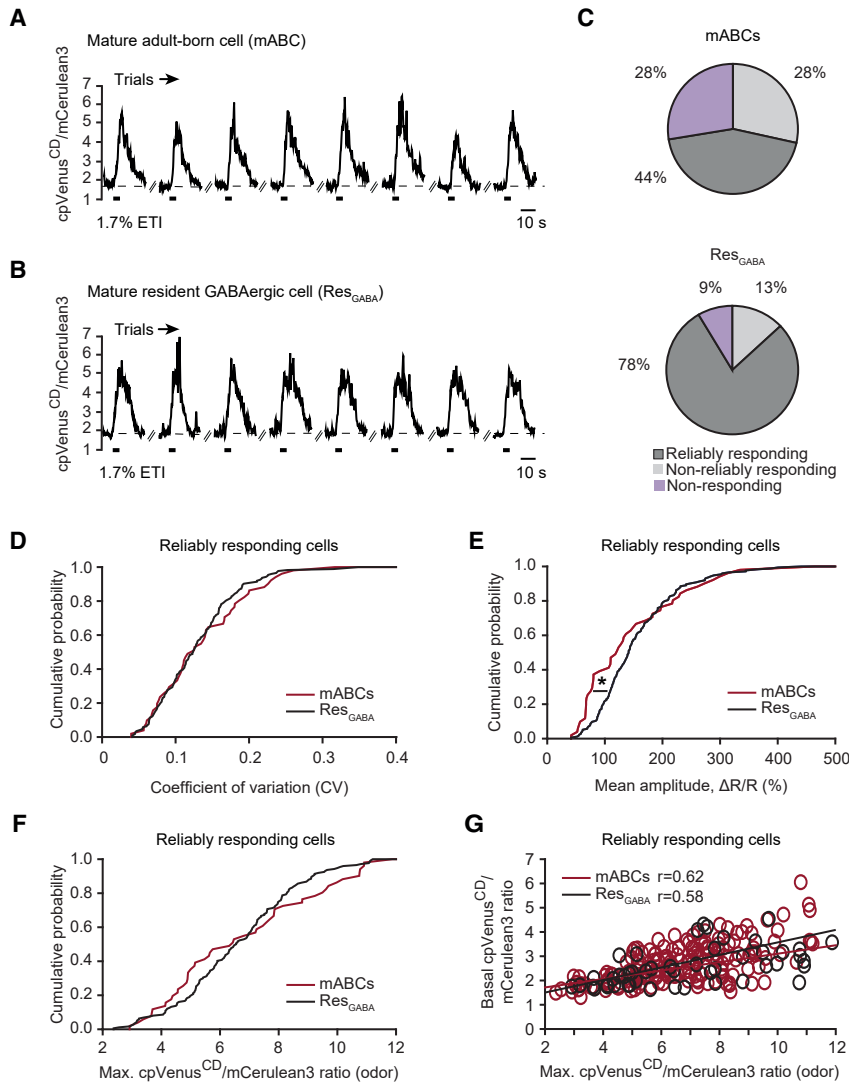


Figure 3. Odor-Evoked Responses of mABC and Res_{GABA} Cells in Awake Mice

(A and B) Sample Ca²⁺ transients evoked by ethyl tiglate (ETI) (1.7% of saturated vapor) in an mABC (A) and a Res_{GABA} cell (B).

(C) Pie charts showing the fractions of reliably responding, non-reliably responding, and non-responding cells among mABCs (top) and Res_{GABA} cells (bottom; $p < 10^{-4}$, chi-square test; $n = 116$ mABCs, 8 mice versus $n = 222$ Res_{GABA} cells, 5 mice).

(D–F) Cumulative probability histograms showing the distributions of the CV (D) ($p = 0.39$, here and below Kolmogorov-Smirnov test, $n = 51$ mABCs, 8 mice versus $n = 174$ Res_{GABA} cells, 5 mice), mean amplitude (E) ($*p = 4 \times 10^{-3}$), and the maximal odor-evoked Twitch-2B ratios (F) ($p = 0.19$).

(G) Relationships between the basal and the maximal odor-evoked Twitch-2B ratios (Spearman's rank correlation coefficient $r = 0.62$, $n = 51$ mABCs; $r = 0.58$, $n = 174$ Res_{GABA} cells, $p < 10^{-4}$ for both comparisons).

Differential Effects of Cholinergic and Serotonergic Receptor Blockers on Basal Ca²⁺ Levels of mABCs and Res_{GABA} Cells in Awake Mice

Because activity of both mABCs and Res_{GABA} cells was significantly reduced under anesthesia, we tested whether centrifugal projections arising from ARAS (ascending reticular activating system) centers (e.g., locus coeruleus, nucleus basalis of Meynert, raphe nuclei) contribute to the neuronal activity observed in awake state and whether these projections target mABCs and Res_{GABA} cells differently. Hence, respective basal Twitch-2B ratios were measured before and during topical applications of noradrenergic (NA), serotonergic (5-hydroxytryptamin [5-HT]), or cholinergic (acetylcholine [ACh]) receptor blockers to the dorsal surface of the OB.

As all blockers were diluted in the HEPES-buffered Ringier's solution, we first assured that this solution does not

change the Twitch-2B ratios (Note S1). The basal ratios of mABCs did not change in the presence of the adrenergic receptor blocker prazosin (Figure 6A), whereas the 5-HT receptor blocker methysergide significantly reduced the basal ratios, decreasing the fraction of spiking and increasing the fraction of non-spiking cells (Figure 6B). Similarly, a mixture of scopolamine/mecamylamine significantly reduced the basal ratios and thus the fraction of spiking cells (Figure 6C). The median (per mouse) effect size for prazosin was 2.28%, for methysergide 47.19%, and for mecamylamine/scopolamine 50.40% ($p = 0.40, 0.03, \text{ and } 0.03$, respectively, one-tailed Wilcoxon signed rank test, $n = 5$ mice; Figure 6D). We did not observe any linear correlation between the effect size of the methysergide-evoked blockade in individual mABCs and the basal Twitch-2B ratios of these cells measured under control conditions

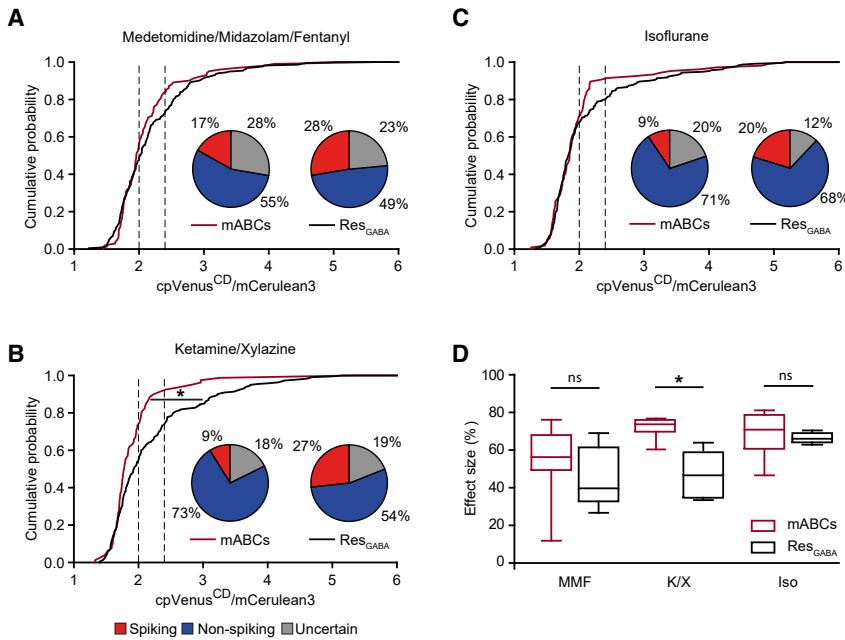


Figure 4. Basal Twitch-2B Ratios of mABCs and Res_{GABA} Cells in Anesthetized Mice

(A–C) Cumulative probability histograms showing the distributions of Twitch-2B ratios under MMF (A), K/X (B), and isoflurane anesthesia (C). The distributions were similar under MMF (A) ($p = 0.24$, $n = 101$ versus 217 cells, here and below Kolmogorov-Smirnov test) or isoflurane (C) ($p = 0.99$, $n = 106$ versus 232 cells) anesthesia but differed significantly under K/X anesthesia (B) ($*p = 1.2 \times 10^{-3}$, $n = 79$ versus 221 cells). Pie charts show the fractions of spiking, non-spiking, and uncertain cells. The fractions were similar under MMF (A) but differed significantly under K/X (B) and isoflurane (C) anesthesia ($p = 0.12$, 3×10^{-3} and 1.6×10^{-2} , respectively, chi-square test). (D) Boxplot shows the median (per mouse) effect sizes for mABCs and Res_{GABA} cells under three anesthesia regimens ($*p < 0.01$, two-way ANOVA with a Bonferroni *post-hoc* test).

(Pearson correlation coefficient $r = 0.08$, $p = 0.69$). This suggests the absence of a larger 5-HT input to highly spontaneously active mABCs.

In Res_{GABA} cells, neither prazosin (Figure 7A) nor methysergide (Figure 7B) reduced the basal Twitch-2B ratios but the ratios were significantly reduced by the ACh receptor blockers (Figure 7C). The median effect size (Figure 7D) for prazosin was 0.53%, for methysergide 6.75%, and for mecamylamine/scopolamine 54.26% ($p = 0.5$, 0.06, and 0.03, respectively, one-tailed Wilcoxon signed rank test, $n = 5$ mice). Thus, the 5-HT receptor blocker affected mABCs and Res_{GABA} cells differently (Figure 7E), whereas the effect sizes of ACh receptor blockers were similar.

DISCUSSION

This study compared the *in vivo* functional properties of mABCs with that of Res_{GABA} cells in awake mice. Several unique functional properties of mABCs distinguished them from Res_{GABA} cells. First, basal Twitch-2B ratios, reflecting the basal levels of $[Ca^{2+}]_i$, were significantly higher in mABCs (Figure 2C), with a unique cluster of highly spontaneously active mABCs (Figure 2E), comprising approximately a quarter of the population. Cells with such high levels of activity were absent among Res_{GABA} cells. Secondly, a significantly smaller fraction of mABCs responded to odorants under awake conditions and 2.2 times as many mABCs as Res_{GABA} cells were non-reliably responding (Figure 3C). Because the reliability of mABC odor responses increased under subsequent anesthesia, we hypothesize that some

waking-specific inhibitory inputs fall away under anesthesia. Consistently, in reliably responding mABCs of awake mice the response amplitudes were significantly smaller compared with those of reliably responding Res_{GABA} cells. Thirdly, mABCs were in general more sensitive to anesthesia, with significantly lower basal Twitch-2B ratios recorded under K/X anesthesia (Figure 4). Finally, in the awake state the ongoing activity of mABCs but not Res_{GABA} cells was strongly driven by 5-HT inputs, as a 5-HT receptor blocker dramatically reduced basal Twitch-2B ratios only in mABCs.

Methodological Considerations

Correct functional comparison of mABCs and Res_{GABA} cells requires that (1) cell populations are compared a long time after they were labeled with a functional marker and (2) the composition of the populations under study is comparable. To fulfill these criteria we used Twitch-2B, which is well tolerated by living cells and does preserve its functional properties *in vivo* for months (Thestrup et al., 2014). As ABCs mature to become GABAergic interneurons, we compared them with resident Vaaat-positive cells, more than 98% of which are GABAergic interneurons (Chao et al., 2010). It has to be noted that neither mABC nor Res_{GABA} cell populations are homogeneous. According to our immunohistochemical data (Figure S2), Res_{GABA} cells studied here comprise 23.6% of tyrosine hydroxylase-, 38.5% of calretinin-, and 19.8% of calbindin-D-28k-positive cells. These results closely match the literature data reporting 16%–21% of tyrosine hydroxylase-, 33%–44% of calretinin-, and 10%–14% of calbindin-D-28k-positive cells among Res_{GABA} cells (Kosaka and Kosaka, 2007;

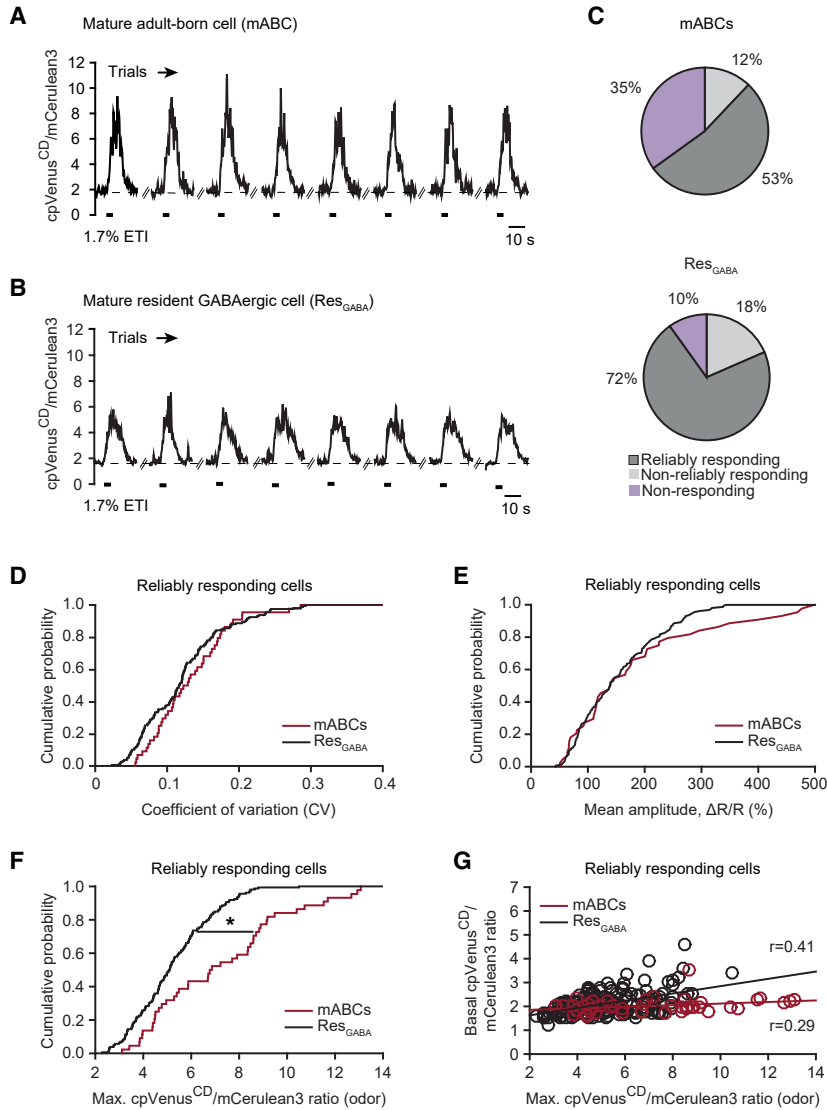


Figure 5. Odor-Evoked Responses of mABCs and Res_{GABA} Cells under MMF Anesthesia

(A and B) Sample Ca²⁺ transients evoked by ETI (1.7% of saturated vapor) in an mABC (A) and a Res_{GABA} cell (B).

(C) Pie charts showing the fractions of reliably responding, non-reliably responding, and non-responding cells among mABCs (top) and Res_{GABA} cells (bottom; $p = 10^{-4}$, chi-square test; $n = 83$ mABCs, 7 mice and 222 Res_{GABA} cells, 5 mice).

(D–F) Cumulative probability histograms showing the distributions of the CV (D) ($p = 0.31$, here and below Kolmogorov-Smirnov test, $n = 44$ and 159 reliably responding cells), the amplitude (E) ($p = 0.46$), and the maximal odor-evoked Twitch-2B ratios (F) ($*p = 8.7 \times 10^{-5}$). (G) Relationships between the basal and the maximal odor-evoked Twitch-2B ratios (mABCs: $r = 0.29$, $p = 5.1 \times 10^{-2}$; Res_{GABA} cells: $r = 0.41$, $p = 10^{-7}$, Spearman’s rank correlation).

Panzanelli et al., 2007; Parrish-Aungst et al., 2007). According to our previous data, mABCs comprise 17.4% of tyrosine hydroxylase-, 37.3% of calretinin-, and 16.2% of calbindin-D-28k-positive cells (Kovalchuk et al., 2015). Despite the above similarity, some differences between mABCs and Res_{GABA} cells still exist. For instance, 2.5% of the dopaminergic Res_{GABA} cells are generated only prenatally and are therefore absent among mABCs (Galliano et al., 2018). Instead, mABCs contain ~5% of glutamatergic neurons (Brill et al., 2009), which are absent among Res_{GABA} cells. Therefore, a small mismatch in the composition of the cell populations is possible but, in our view, it cannot explain the population-wide functional differences observed in this study.

Furthermore, we used lentiviruses to label mABCs. Although providing superior cell brightness, this is “a

somewhat ‘noisy’ method with regard to precise birth dating” (Livneh and Mizrahi, 2011). Indeed, 5.5% of mABCs in our study were doublecortin-positive and thus likely younger than their nominal age. However, the known properties of young ABCs are opposite to the herein described properties of mABCs. Whereas mABCs show higher basal Twitch-2B ratios compared with resident cells, reflecting their high spontaneous firing rate (Figures 1, 2, and S1), the spontaneous firing rate of ABCs at 9–28 days post-injection is much lower than that of resident cells (Kovalchuk et al., 2015; Livneh et al., 2014). Secondly, immature ABCs have higher odor responsiveness compared with resident cells (see Figures 3B and 3D in Livneh et al., 2014), whereas mABCs have significantly lower odor responsiveness (Figure 3C). Finally, the amplitudes of odor-evoked

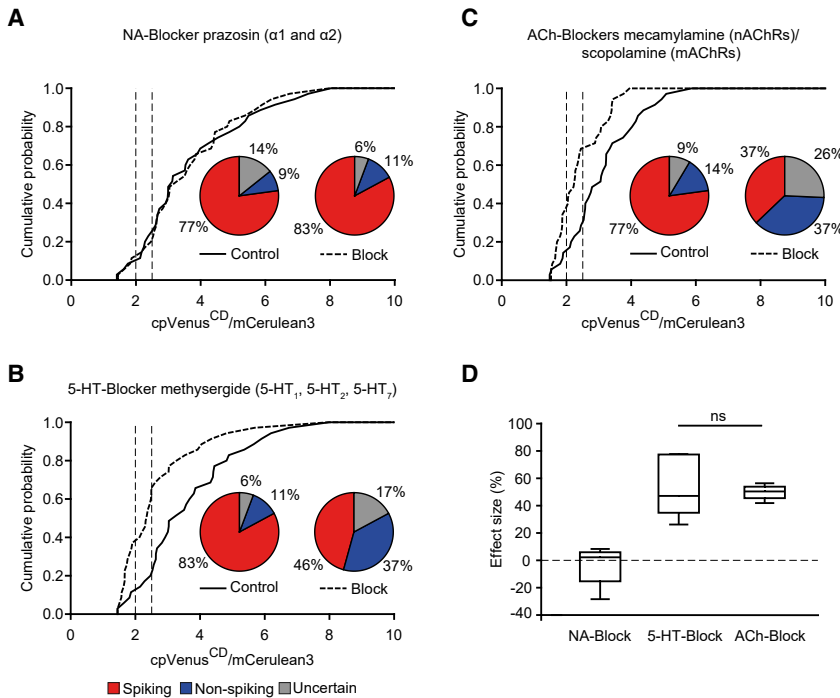


Figure 6. Effect of Receptor Blockers on Basal Twitch-2B Ratios of mABCs in Awake Mice

(A–C) Cumulative probability histograms showing the distributions of basal Twitch-2B ratios in control and during topical application of prazosin (A), methysergide (B), and mecamlamine/scopolamine (C). Pie charts (A–C, insets) show the fractions of spiking, non-spiking, and uncertain cells under two conditions. Prazosin had no effect (A) ($p = 0.37$; here and below McNemar-Bowker test, $n = 35$ cells, 5 mice) but methysergide (B) ($p = 3 \times 10^{-3}$) and mecamlamine/scopolamine (C) ($p = 2 \times 10^{-3}$) changed the fractions significantly.

(D) Boxplot showing the median (per mouse) effect sizes for different receptor blockers (5-HT versus ACh receptor blockers: $p = 0.81$, Wilcoxon signed rank test).

signals of immature ABCs are higher compared with resident cells (see Figure 3C in Livneh et al., 2014), whereas in our study, the amplitudes of >60% of mABCs are significantly lower (Figure 3E). These data strongly suggest that the use of lentivirus-based cell labeling, if anything, underestimates the differences between mABCs and Res_{GABA} reported in the present study.

Ongoing Activity of GABAergic Juxtglomerular Neurons

The use of the ratiometric Ca²⁺ indicator allowed to visualize the ongoing spontaneous activity of JGCs. Only 18%–25% of JGCs were non-spiking, whereas the vast majority of both resident and adult-born JGCs were active in awake state. JGCs thus impose a strong ongoing inhibitory drive on their synaptic partners. Interestingly, 24.1% of mABCs had very high basal Twitch-2B ratios, likely caused by ongoing spontaneous activity and AP firing (Figure 1D). Such a subpopulation was absent among Res_{GABA} cells. Previously, the ongoing spontaneous activity was reported for “many” OB GCs in awake mice (Kato et al., 2012) but was not described by the same authors for the population of parvalbumin-positive interneurons located in the external plexiform layer (Kato et al., 2013). However, the use of a non-ratiometric Ca²⁺ indicator in previous studies allowed to visualize fluctuations of ongoing activity rather than its steady-state level (see also Figure 3 in Homma et al., 2013).

All three anesthesia regimens used in our study significantly reduced the ongoing spontaneous activity in JGCs, suggesting that this effect is caused by the change in brain state. Under anesthesia, the fraction of silent Res_{GABA} cells roughly doubled, while that of silent mABCs increased by ~3.5-fold. However, approximately 25% of Res_{GABA} cells remained active, in contrast to OB GCs, showing little spontaneous activity both under urethane/chlorprothixene and K/X anesthesia (Kato et al., 2012). Consistent with our data, low-resolution imaging of population activity in GAD2-Cre and TH-Cre mice, in which either PGCs or SACs are selectively labeled, revealed an isoflurane-induced decrease in resting GCaMP3 fluorescence by approximately 20% (Wachowiak et al., 2013).

For ketamine/xylazine, the extent of the anesthetic-mediated blockade was significantly stronger for mABCs compared with Res_{GABA} cells (Figures 4D and S5). This effect is likely caused by the NMDA receptor blocker ketamine, because xylazine acts alike the MMF anesthesia component medetomidine and MMF anesthesia had a similar effect on mABCs and Res_{GABA} cells. In ABCs, NMDA receptors are important for differentiation, synaptic development, maturation of glutamatergic synapses, and long-term cell survival (Kelsch et al., 2012; Lin et al., 2010; Platel and Kelsch, 2013; Tashiro et al., 2006). NMDA receptors are thought to underlie the heightened synaptic plasticity of ABCs, which is restricted to the critical period of ABC development (age 4–8 weeks; Ge et al., 2007; Tashiro et al., 2006). Our data

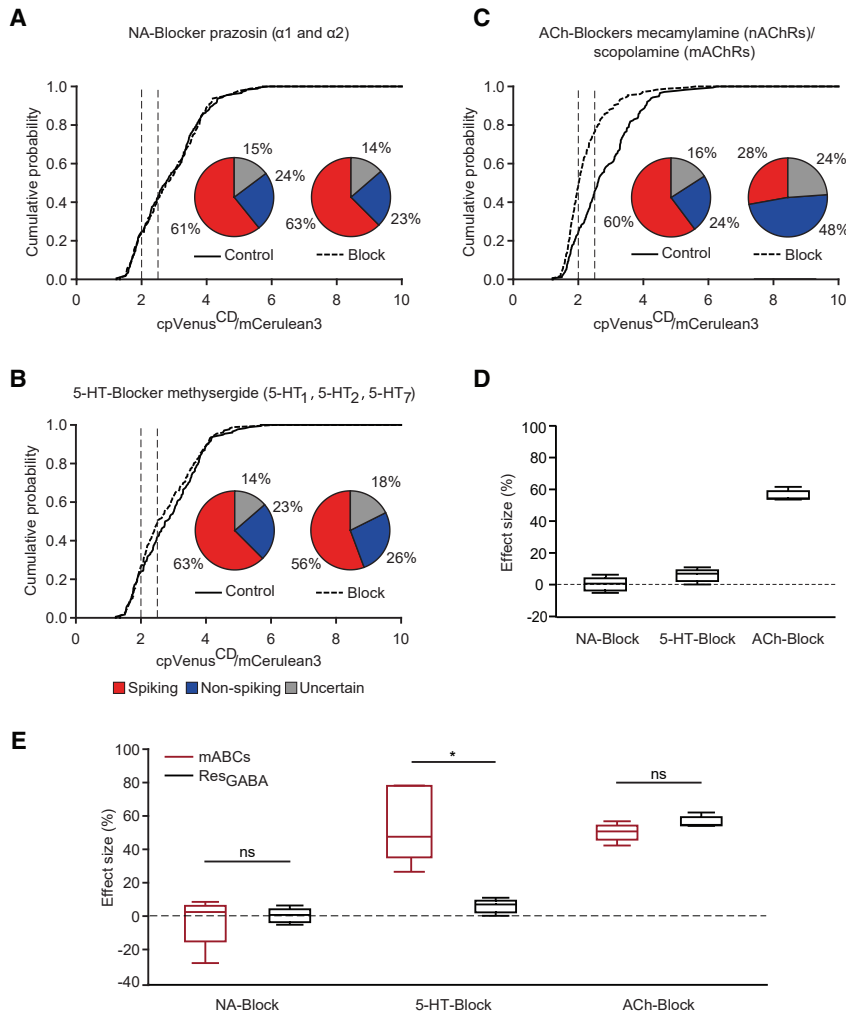


Figure 7. Effect of Receptor Blockers on Basal Twitch-2B Ratios of Res_{GABA} Cells in Awake Mice

(A–C) Cumulative probability histograms showing the distributions of the basal Twitch-2B ratios in control and during topical application of prazosin (A), methysergide (B), and mecamlamine/scopolamine (C). Pie charts (A–C, insets) show the fractions of spiking, non-spiking, and uncertain cells. Prazosin (A) ($p = 0.51$, here and below McNemar-Bowker test, $n = 176$ cells, 5 mice) and methysergide (B) ($p = 0.11$) had no effect, but mecamlamine/scopolamine changed the fractions significantly (C) ($p < 10^{-3}$). (D) Boxplot shows the median (per mouse) effect sizes for different receptor blockers. (E) Comparison of median (per mouse) effect sizes between mABCs and Res_{GABA} cells. There was a significant difference for methysergide ($*p < 10^{-3}$, two-way ANOVA with a Bonferroni *post-hoc* test).

suggest that also after this period ABCs preserve the heightened levels of NMDA receptor activity.

Odor-Evoked Responsiveness of GABAergic Juxtglomerular Cells

In contrast to the robust spontaneous activity of mABCs, their ETI-evoked responses in the awake state involved fewer cells, and were weaker and much less reliable than those of Res_{GABA} cells. However, the response reliability in the very same mABCs improved under the anesthesia. Thus, the lack of reliability in the awake state cannot be explained by the fewer connections to the synaptic partners, i.e., weaker integration of these cells into the surrounding network. Rather, it is either due to a specific inhibitory input active only in the awake state or to a specific excitatory input active under the anesthesia. The majority of PGCs and SACs receive their olfactory input indirectly, via glutamatergic external tufted (Kiyokage et al., 2010) or M/T cells (Lledo et al., 2008). Furthermore, OB glutamatergic cells seem to be less sensitive

to anesthesia compared with GABAergic cells (Kato et al., 2012; Rinberg et al., 2006; Wachowiak et al., 2013). Thus, an increase in the reliability of odor-evoked responses in mABCs could be explained by the anesthesia-induced relative increase in the excitation/inhibition ratio. In any case, in the awake state mABCs are unlikely to play the major role for the reliable feedforward inhibition of odor-evoked responses in M/T cells as they are responding less. According to our data, this role is much better fulfilled by Res_{GABA} cells.

Neuromodulatory Inputs to Juxtglomerular Neurons

This is the first study analyzing the influence of ARAS-related neuromodulators on the ongoing activity of the adult-born and resident JGCs in the awake state. In line with anatomical data showing that noradrenergic projections from the locus coeruleus terminate in all but the most superficial layers of the OB (Devore and Linster, 2012; Gomez et al., 2005), the adrenergic receptor blocker had little effect on the ongoing activity of JGCs (Figures 6 and 7). We have, however,



observed a strong effect of the ACh receptor blockers. Also these data are consistent with the anatomy of the cholinergic projections from the basal forebrain, known to innervate primarily glomerular and GC layers (Devore and Linster, 2012; Gomez et al., 2005). While in single unit recordings in anesthetized rats (Ravel et al., 1990) iontophoretic application of ACh elicited both excitatory and inhibitory responses, in our hands the effect of endogenous ACh was clearly excitatory as its blockade roughly doubled the fraction of non-spiking JGCs. However, the effects of ACh blockers, and hence also the density of functional cholinergic projections synapsing on mABCs and Res_{GABA} cells, were similar, suggesting that in the awake state both cell types are working on the same common project. Experiments in anesthetized rats (Chaudhury et al., 2009) as well as computational analyses (Devore and Linster, 2012) suggested that endogenous cholinergic activation of these cells might contribute to amplitude-invariant processing of odor-evoked signals, decorrelation of odor representations and an increase in perceptual discrimination between chemically similar odorants.

The Unique Serotonergic Innervation of mABCs

The 5-HT inputs to the OB arise from the dorsal raphe nucleus and predominantly target the GL (Gomez et al., 2005; McLean and Shipley, 1987). They inhibit inputs from the nose, partly via JGC-mediated presynaptic inhibition (Petzold et al., 2009; Wachowiak et al., 2009). Consistently, in awake mice the ongoing spontaneous activity of mABCs was blocked by methysergide (Figure 6B), suggesting that 5-HT inputs do sustain the ongoing inhibition that these cells impose on their synaptic partners. Strikingly, the sensitivity to methysergide, one of the most potent modulators of the presynaptic odor-evoked responses (Petzold et al., 2009), represented a unique feature of mABCs and was barely seen in Res_{GABA} cells (Figure 7E), suggesting that this important function is fulfilled by adult-born JGCs. Because the activity of 5-HT neurons is brain state dependent with high activity levels during awake resting but not during attentive states of sensory acquisition (Jacobs and Azmitia, 1992; Jones, 2005), the mABC-mediated presynaptic inhibition is likely to be brain state specific, actively inhibiting the OB inputs during rest and releasing the inhibition during focused attention. These data support the hypothesis that ABCs function as coincidence detectors between the behavioral state of the animal (e.g., arousal, attention, expectation) and sensory inputs arising from the environment (Lazarini and Lledo, 2011).

Interestingly, 5-HT modulates the fate and the functional state of ABCs throughout the entire life. It promotes proliferation of progenitor cells in the SVZ (Banasr et al., 2004; Brezun and Daszuta, 1999), controls the velocity and the directionality of ABC migration in the RMS (Garcia-Gonzalez et al., 2017), and likely influences the survival of these

cells in the OB (Soumier et al., 2010). Here, we show that ABCs do preserve their privileged 5-HT inputs even after integration into the OB circuitry and maturation therein.

In conclusion, our study is the first to describe the *in vivo* functional properties of mature adult-born JGCs in awake mice, showing that even under control conditions these properties are different from those of Res_{GABA} cells. Together with data of Livneh et al. (2014), showing that ABCs can acquire distinct properties when developing in the odor-enriched environment, our data firmly identify mABCs as a neuronal population with distinct and maybe even unique functions.

EXPERIMENTAL PROCEDURES

Animals

Experiments were conducted in accordance with biometrical planning/institutional animal welfare guidelines and were approved by the state government of Baden-Württemberg, Germany. C57BL/6 (WT, Charles River) and B6.FVB-Tg(Slc32a1-cre)2.1Hzo/TrkJ (Viat-Cre bred on the C57BL/6 background, Jackson Laboratory) mice of either sex were used to study mABCs and Res_{GABA} cells, respectively. Animals were kept in pathogen-free conditions at 22°C, 60% air humidity, 12-h light/dark cycle, with *ad libitum* access to food and water. Females stayed in groups of three to five mice, males were kept individually.

Expression of Twitch-2B in mABCs and Res_{GABA} Cells

To label ABCs, house-made lentiviral (Note S2) vectors (1.5 μ L, 1×10^8 infectious units/mL; Maslyukov et al., 2018) encoding the Ca²⁺ indicator Twitch-2B under the ubiquitin promoter were stereotactically injected (3.0 mm anterior, 0.84 mm lateral from bregma, and 2.9 mm ventral from dura) into the RMS of adult WT mice. By the time studied, only $5.5\% \pm 6.7\%$ (median \pm SEM, $n = 448$ cells, 5 mice) of Twitch-2B-expressing mABCs also expressed doublecortin, a marker for immature neurons.

To label Res_{GABA} cells, adeno-associated virus (1×10^{13} infectious units/mL, 1 μ L of 1:7 diluted solution) encoding a Cre-inducible version of Twitch-2B under control of the CAG promoter (AAV1.CAG.Flex.Twitch2B.WPRE.SV40, Addgene 49531M; Penn Vector Core, Philadelphia, PA) was injected into the dorsal OB (at 0.35, 0.25, and 0.15 mm depth, ~ 300 nL per injection) of 1-month-old Viat-Cre mice at an 45° angle from the horizontal plane.

In Vivo Two-Photon Ca²⁺ Imaging

Mature ABCs (3.5 ± 1.6 months post-injection) and Res_{GABA} cells (8.9 ± 1.6 months post-injection) were imaged in awake/anesthetized animals (aged 7.6 ± 1.9 and 9.8 ± 1.6 months, respectively). Before awake imaging, mice were habituated to the setup for ~ 12 days by daily fixations, lasting 5 min (at the beginning) to 60 min (at the end of training).

For anesthesia induction, mice were sedated with isoflurane (1–2 min, 2.5% in O₂) and then injected intraperitoneally with either K/X or MME. The breathing rate was monitored with a pressure sensor (ADInstruments, Spechbach, Germany) attached to the



back. For isoflurane anesthesia, it was kept at 100–130 breaths/min by adjusting the isoflurane concentration (0.9%–1.5% in O₂). Recordings commenced 10 min after anesthesia induction.

We used an Olympus FluoView 1000 laser scanning system coupled to a mode-locked Ti:Sapphire laser (Mai Tai DeepSee, Spectra-Physics, Germany). Twitch-2B was excited at 890 nm and imaged using a 20× UMPlan FI 1.0 NA water-immersion objective (Zeiss). Fluorescence of mCerulean3 and cpVenus^{CD} was separated using a 515-nm dichroic mirror and a 475/64-nm band pass and 500-nm-long pass filters, respectively. Time series were recorded at 4–8 Hz. In some experiments, basal Twitch-2B ratios were derived from single frames of Z series. Z series were acquired at a depth of 10–120 μm: image size, 640 × 640 pixels; Kalman filter, 2; and step size, 2 μm.

ETI (Sigma-Aldrich) was applied to the mouse snout using a custom-built flow dilution olfactometer at a flow rate of 300 mL/min (Homma et al., 2013). The odorant was delivered eight times for 4 s per trial with an inter-trial interval of 1–2 min.

Application of Receptor Blockers in Awake Mice

Blockers were dissolved in HEPES-buffered Ringer's solution (Note S1). Prazosin, methysergide, scopolamine, and mecamlamine were applied at final concentrations of 100 μM, and 4, 50, and 115 mM, respectively.

Data Analyses

The regions of interest (ROIs) covering cell somata were drawn manually in ImageJ 8 (<https://imagej.nih.gov/ij>), the background ROI had a comparable size. Further analyses used Custom written MATLAB scripts (The MathWorks). The ratio was calculated as

$$\text{Ratio} = \frac{m\text{Cerulean3} - m\text{Cerulean3}_{\text{background}}}{cp\text{Venus}^{\text{CD}} - cp\text{Venus}^{\text{CD}}_{\text{background}}} \quad (\text{Equation 1})$$

using the mean ROI intensities measured in the respective channels.

Basal ratios are averages of all ratio values measured in a single time-series recording in the absence of any exogenous stimuli. Time points of recording were chosen randomly, no selection based on cell's instant activity pattern or any other criteria was performed.

Maximal ratios (R_{max}) of the odor-evoked Ca²⁺ transients were measured 0–6 s after odor stimulus onset, after smoothing the ratio trace twice with the 0.3-s time window binomial filter.

ΔR/R was calculated as follows:

$$\frac{\Delta R}{R} (\%) = \frac{\text{Ratio} - \text{Ratio}_{\text{baseline}}}{\text{Ratio}_{\text{baseline}}} * 100,$$

where *Ratio* is the trace calculated according to (1) and *Ratio*_{baseline} is a mean ratio measured 1–5 s before the onset of the odor stimulus.

Odor-evoked signals were scored as responses when the signal amplitude was at least 15% of ΔR/R and six times larger than the SD of the corresponding baseline noise. The CV was calculated as follows:

$$\text{CV} = \frac{SD}{\bar{x}} * \left(1 + \frac{1}{4 * n}\right),$$

where SD is the standard deviation of R_{max}, \bar{x} is the mean R_{max} of the successful trials, and n is the number of successful trials. The part in parentheses is the correction for the small sample size.

The effect size was calculated as:

$$\text{effect size} (\%) = \frac{R_{\text{ctr}} - R_{\text{test}}}{R_{\text{ctr}} - R_{\text{min}}} * 100,$$

where R_{ctr} and R_{test} are the cell's ratios measured under control and test conditions, respectively, R_{min} = 1.25 is the lowest ratio ever observed in our recordings. R_{test} = R_{min} was considered as a 100% block of cell activity. As activity can be blocked in spiking cells only, the effect size was calculated only for cells with ratios >2.4.

Statistical Analyses

Two-sided statistical tests were done using MATLAB, GraphPad Prism (www.graphpad.com), SPSS, or Vassar Stats (<http://vassarstats.net/>). Normality of the data distribution was tested with a one-sample Kolmogorov-Smirnov test. p values < 0.05 were considered significant. Unless indicated, data are presented as median ± IQR.

Data and Code Availability

All data of this study are reported in the main text and Supplemental Information. In-house MATLAB scripts and the raw imaging files are available from the corresponding author upon reasonable request.

SUPPLEMENTAL INFORMATION

Supplemental Information can be found online at <https://doi.org/10.1016/j.stemcr.2020.10.010>.

AUTHOR CONTRIBUTIONS

O.G. conceived the study. N.F.-T., Y.K., S.F., N.M., E.Z., and A.A. performed the experiments and/or data analyses. N.F.-T. and O.G. wrote the manuscript and all authors approved the manuscript.

ACKNOWLEDGMENTS

We thank A. Weible and K. Schöntag for technical assistance; Y. Liang and W. Pflöging (Institute for Applied Materials, Karlsruhe, Germany) for help with topical drug application; X. Su, K. Li, N. Asavapanumas, and M. E. Schmidt for help with experiments/ data analyses. This work was supported by the Deutsche Forschungsgemeinschaft (DFG) grant no. GA 654/14-1 (to O.G.).

Received: May 4, 2020

Revised: October 20, 2020

Accepted: October 21, 2020

Published: November 19, 2020

REFERENCES

Alonso, M., Viollet, C., Gabellec, M.M., Meas-Yedid, V., Olivo-Marin, J.C., and Lledo, P.M. (2006). Olfactory discrimination



- learning increases the survival of adult-born neurons in the olfactory bulb. *J. Neurosci.* 26, 10508–10513.
- Banasr, M., Hery, M., Printemps, R., and Daszuta, A. (2004). Serotonin-induced increases in adult cell proliferation and neurogenesis are mediated through different and common 5-HT receptor subtypes in the dentate gyrus and the subventricular zone. *Neuropsychopharmacol* 29, 450–460.
- Bauer, S., Moyses, E., Jourdan, F., Colpaert, F., Martel, J.C., and Marien, M. (2003). Effects of the α 2-adrenoreceptor antagonist dexefaroxan on neurogenesis in the olfactory bulb of the adult rat in vivo: selective protection against neuronal death. *Neurosci* 117, 281–291.
- Belluzzi, O., Benedusi, M., Ackman, J., and LoTurco, J.J. (2003). Electrophysiological differentiation of new neurons in the olfactory bulb. *J. Neurosci.* 23, 10411–10418.
- Brezun, J.M., and Daszuta, A. (1999). Depletion in serotonin decreases neurogenesis in the dentate gyrus and the subventricular zone of adult rats. *Neurosci* 89, 999–1002.
- Brill, M.S., Ninkovic, J., Winpenny, E., Hodge, R.D., Ozen, I., Yang, R., Lepier, A., Gascon, S., Erdelyi, F., Szabo, G., et al. (2009). Adult generation of glutamatergic olfactory bulb interneurons. *Nat. Neurosci.* 12, 1524–1533.
- Chao, H.T., Chen, H., Samaco, R.C., Xue, M., Chahrouh, M., Yoo, J., Neul, J.L., Gong, S., Lu, H.C., Heintz, N., et al. (2010). Dysfunction in GABA signalling mediates autism-like stereotypies and Rett syndrome phenotypes. *Nature* 468, 263–269.
- Chaudhury, D., Escanilla, O., and Linster, C. (2009). Bulbar acetylcholine enhances neural and perceptual odor discrimination. *J. Neurosci.* 29, 52–60.
- Deshpande, A., Bergami, M., Ghanem, A., Conzelmann, K.K., Lepier, A., Gotz, M., and Berninger, B. (2013). Retrograde monosynaptic tracing reveals the temporal evolution of inputs onto new neurons in the adult dentate gyrus and olfactory bulb. *Proc. Natl. Acad. Sci. U S A* 110, E1152–E1161.
- Devore, S., and Linster, C. (2012). Noradrenergic and cholinergic modulation of olfactory bulb sensory processing. *Front. Behav. Neurosci.* 6, 52.
- Feierstein, C.E., Lazarini, F., Wagner, S., Gabellec, M.M., de Chaumont, F., Olivo-Marin, J.C., Boussin, F.D., Lledo, P.M., and Gheusi, G. (2010). Disruption of adult neurogenesis in the olfactory bulb affects social interaction but not maternal behavior. *Front. Behav. Neurosci.* 4, 176.
- Galliano, E., Franzoni, E., Breton, M., Chand, A.N., Byrne, D.J., Murthy, V.N., and Grubb, M.S. (2018). Embryonic and postnatal neurogenesis produce functionally distinct subclasses of dopaminergic neuron. *eLife* 7, 1–36.
- Garcia-Gonzalez, D., Khodosevich, K., Watanabe, Y., Rollenhagen, A., Lubke, J.H.R., and Monyer, H. (2017). Serotonergic projections govern postnatal neuroblast migration. *Neuron* 94, 534–549 e539.
- Ge, S., Yang, C.H., Hsu, K.S., Ming, G.L., and Song, H. (2007). A critical period for enhanced synaptic plasticity in newly generated neurons of the adult brain. *Neuron* 54, 559–566.
- Gomez, C., Brinon, J.G., Barbado, M.V., Weruaga, E., Valero, J., and Alonso, J.R. (2005). Heterogeneous targeting of centrifugal inputs to the glomerular layer of the main olfactory bulb. *J. Chem. Neuroanat.* 29, 238–254.
- Grubb, M.S., Nissant, A., Murray, K., and Lledo, P.M. (2008). Functional maturation of the first synapse in olfaction: development and adult neurogenesis. *J. Neurosci.* 28, 2919–2932.
- Homma, R., Kovalchuk, Y., Konnerth, A., Cohen, L.B., and Garaschuk, O. (2013). In vivo functional properties of juxtglomerular neurons in the mouse olfactory bulb. *Front. Neural Circuit* 7, 23.
- Jacobs, B.L., and Azmitia, E.C. (1992). Structure and function of the brain serotonin system. *Physiol. Rev.* 72, 165–229.
- Jones, B.E. (2005). From waking to sleeping: neuronal and chemical substrates. *Trends Pharmacol. Sci.* 26, 578–586.
- Kaneko, N., Okano, H., and Sawamoto, K. (2006). Role of the cholinergic system in regulating survival of newborn neurons in the adult mouse dentate gyrus and olfactory bulb. *Genes Cells* 11, 1145–1159.
- Kato, H.K., Chu, M.W., Isaacson, J.S., and Komiyama, T. (2012). Dynamic sensory representations in the olfactory bulb: modulation by wakefulness and experience. *Neuron* 76, 962–975.
- Kato, H.K., Gillet, S.N., Peters, A.J., Isaacson, J.S., and Komiyama, T. (2013). Parvalbumin-expressing interneurons linearly control olfactory bulb output. *Neuron* 80, 1218–1231.
- Kelsch, W., Li, Z., Eliava, M., Goengrich, C., and Monyer, H. (2012). GluN2B-containing NMDA receptors promote wiring of adult-born neurons into olfactory bulb circuits. *J. Neurosci.* 32, 12603–12611.
- Kiyokage, E., Pan, Y.Z., Shao, Z., Kobayashi, K., Szabo, G., Yanagawa, Y., Obata, K., Okano, H., Toida, K., Puche, A.C., et al. (2010). Molecular identity of periglomerular and short axon cells. *J. Neurosci.* 30, 1185–1196.
- Kosaka, K., and Kosaka, T. (2007). Chemical properties of type 1 and type 2 periglomerular cells in the mouse olfactory bulb are different from those in the rat olfactory bulb. *Brain Res.* 1167, 42–55.
- Kovalchuk, Y., Homma, R., Liang, Y., Maslyukov, A., Hermes, M., Thestrup, T., Griesbeck, O., Ninkovic, J., Cohen, L.B., and Garaschuk, O. (2015). In vivo odourant response properties of migrating adult-born neurons in the mouse olfactory bulb. *Nat. Commun.* 6, 6349.
- Lazarini, F., and Lledo, P.M. (2011). Is adult neurogenesis essential for olfaction? *Trends Neurosci.* 34, 20–30.
- Li, W.L., Chu, M.W., Wu, A., Suzuki, Y., Imayoshi, I., and Komiyama, T. (2018). Adult-born neurons facilitate olfactory bulb pattern separation during task engagement. *eLife* 7. <https://doi.org/10.7554/eLife.33006.014>.
- Liang, Y., Li, K., Riecken, K., Maslyukov, A., Gomez-Nicola, D., Kovalchuk, Y., Fehse, B., and Garaschuk, O. (2016). Long-term in vivo single-cell tracking reveals the switch of migration patterns in adult-born juxtglomerular cells of the mouse olfactory bulb. *Cell Res.* 26, 805–821.
- Lin, C.W., Sim, S., Ainsworth, A., Okada, M., Kelsch, W., and Lois, C. (2010). Genetically increased cell-intrinsic excitability enhances neuronal integration into adult brain circuits. *Neuron* 65, 32–39.



- Livneh, Y., Adam, Y., and Mizrahi, A. (2014). Odor processing by adult-born neurons. *Neuron* *81*, 1097–1110.
- Livneh, Y., Feinstein, N., Klein, M., and Mizrahi, A. (2009). Sensory input enhances synaptogenesis of adult-born neurons. *J. Neurosci.* *29*, 86–97.
- Livneh, Y., and Mizrahi, A. (2011). Long-term changes in the morphology and synaptic distributions of adult-born neurons. *J. Comp. Neurol.* *519*, 2212–2224.
- Lledo, P.M., Merkle, F.T., and Alvarez-Buylla, A. (2008). Origin and function of olfactory bulb interneuron diversity. *Trends Neurosci.* *31*, 392–400.
- Magavi, S.S., Mitchell, B.D., Szentirmai, O., Carter, B.S., and Macklis, J.D. (2005). Adult-born and preexisting olfactory granule neurons undergo distinct experience-dependent modifications of their olfactory responses in vivo. *J. Neurosci.* *25*, 10729–10739.
- Mak, G.K., Enwere, E.K., Gregg, C., Pakarainen, T., Poutanen, M., Huhtaniemi, I., and Weiss, S. (2007). Male pheromone-stimulated neurogenesis in the adult female brain: possible role in mating behavior. *Nat. Neurosci.* *10*, 1003–1011.
- Maslyukov, A., Li, K., Su, X., Kovalchuk, Y., and Garaschuk, O. (2018). Spontaneous calcium transients in the immature adult-born neurons of the olfactory bulb. *Cell Calcium* *74*, 43–52.
- McLean, J.H., and Shipley, M.T. (1987). Serotonergic afferents to the rat olfactory bulb: origins and laminar specificity of serotonergic inputs in the adult rat. *J. Neurosci.* *7*, 3016–3028.
- Mechawar, N., Saghatelian, A., Grailhe, R., Scoriels, L., Gheusi, G., Gabellec, M.M., Lledo, P.M., and Changeux, J.P. (2004). Nicotinic receptors regulate the survival of newborn neurons in the adult olfactory bulb. *Proc. Natl. Acad. Sci. U S A* *101*, 9822–9826.
- Mizrahi, A. (2007). Dendritic development and plasticity of adult-born neurons in the mouse olfactory bulb. *Nat. Neurosci.* *10*, 444–452.
- Moreno, M.M., Linster, C., Escanilla, O., Sacquet, J., Didier, A., and Madaïron, N. (2009). Olfactory perceptual learning requires adult neurogenesis. *Proc. Natl. Acad. Sci. U S A* *106*, 17980–17985.
- Palmer, A.E., and Tsien, R.Y. (2006). Measuring calcium signaling using genetically targetable fluorescent indicators. *Nat. Protoc.* *1*, 1057–1065.
- Pan, Y.W., Kuo, C.T., Storm, D.R., and Xia, Z. (2012). Inducible and targeted deletion of the ERK5 MAP kinase in adult neurogenic regions impairs adult neurogenesis in the olfactory bulb and several forms of olfactory behavior. *PLoS One* *7*, e49622.
- Panzanelli, P., Fritschy, J.M., Yanagawa, Y., Obata, K., and Sassoè-Pognetto, M. (2007). GABAergic phenotype of periglomerular cells in the rodent olfactory bulb. *J. Comp. Neurol.* *502*, 990–1002.
- Parrish-Aungst, S., Shipley, M.T., Erdelyi, F., Szabo, G., and Puche, A.C. (2007). Quantitative analysis of neuronal diversity in the mouse olfactory bulb. *J. Comp. Neurol.* *501*, 825–836.
- Petreanu, L., and Alvarez-Buylla, A. (2002). Maturation and death of adult-born olfactory bulb granule neurons: role of olfaction. *J. Neurosci.* *22*, 6106–6113.
- Petzold, G.C., Hagiwara, A., and Murthy, V.N. (2009). Serotonergic modulation of odor input to the mammalian olfactory bulb. *Nat. Neurosci.* *12*, 784–791.
- Platel, J.C., and Kelsch, W. (2013). Role of NMDA receptors in adult neurogenesis: an ontogenetic (re)view on activity-dependent development. *Cell. Mol. Life Sci.* *70*, 3591–3601.
- Ravel, N., Akaoka, H., Gervais, R., and Chouvet, G. (1990). The effect of acetylcholine on rat olfactory bulb unit activity. *Brain Res. Bull.* *24*, 151–155.
- Rinberg, D., Koulakov, A., and Gelperin, A. (2006). Sparse odor coding in awake behaving mice. *J. Neurosci.* *26*, 8857–8865.
- Rokni, D., Hemmelder, V., Kapoor, V., and Murthy, V.N. (2014). An olfactory cocktail party: figure-ground segregation of odorants in rodents. *Nat. Neurosci.* *17*, 1225.
- Sakamoto, M., Imayoshi, I., Ohtsuka, T., Yamaguchi, M., Mori, K., and Kageyama, R. (2011). Continuous neurogenesis in the adult forebrain is required for innate olfactory responses. *Proc. Natl. Acad. Sci. U S A* *108*, 8479–8484.
- Siopi, E., Denizet, M., Gabellec, M.M., de Chaumont, F., Olivio-Marin, J.C., Guilloux, J.P., Lledo, P.M., and Lazarini, F. (2016). Anxiety- and depression-like states lead to pronounced olfactory deficits and impaired adult neurogenesis in mice. *J. Neurosci.* *36*, 518–531.
- Soumier, A., Banasr, M., Kerkerian-Le Goff, L., and Daszuta, A. (2010). Region- and phase-dependent effects of 5-HT(1A) and 5-HT(2C) receptor activation on adult neurogenesis. *Eur. Neuropsychopharmacol.* *20*, 336–345.
- Sultan, S., Madaïron, N., Kermen, F., Garcia, S., Sacquet, J., and Didier, A. (2010). Learning-dependent neurogenesis in the olfactory bulb determines long-term olfactory memory. *FASEB J.* *24*, 2355–2363.
- Tashiro, A., Sandler, V.M., Toni, N., Zhao, C., and Gage, F.H. (2006). NMDA-receptor-mediated, cell-specific integration of new neurons in adult dentate gyrus. *Nature* *442*, 929–933.
- Thestrup, T., Litzlbauer, J., Bartholomäus, I., Mues, M., Russo, L., Dana, H., Kovalchuk, Y., Liang, Y., Kalamakis, G., Laukat, Y., et al. (2014). Optimized ratiometric calcium sensors for functional in vivo imaging of neurons and T lymphocytes. *Nat. Meth.* *11*, 175–182.
- Valley, M.T., Mullen, T.R., Schultz, L.C., Sagdullaev, B.T., and Firestein, S. (2009). Ablation of mouse adult neurogenesis alters olfactory bulb structure and olfactory fear conditioning. *Front. Neurosci.* *3*, 51.
- Wachowiak, M., Economo, M.N., Diaz-Quesada, M., Brunert, D., Wesson, D.W., White, J.A., and Rothermel, M. (2013). Optical dissection of odor information processing in vivo using GCaMPs expressed in specified cell types of the olfactory bulb. *J. Neurosci.* *33*, 5285–5300.
- Wachowiak, M., Wesson, D.W., Pirez, N., Verhagen, J.V., and Carey, R.M. (2009). Low-level mechanisms for processing odor information in the behaving animal. *Ann. NY. Acad. Sci. U S A* *1170*, 286–292.
- Wallace, J.L., Wienisch, M., and Murthy, V.N. (2017). Development and refinement of functional properties of adult-born neurons. *Neuron* *96*, 883–896.



Whitman, M.C., and Greer, C.A. (2007). Synaptic integration of adult-generated olfactory bulb granule cells: basal axodendritic centrifugal input precedes apical dendrodendritic local circuits. *J. Neurosci.* *27*, 9951–9961.

Yamaguchi, M., and Mori, K. (2005). Critical period for sensory experience-dependent survival of newly generated granule cells in the adult mouse olfactory bulb. *Proc. Natl. Acad. Sci. U S A* *102*, 9697–9702.